Morphological Zones and Orientation in Injection-Molded Polyethylene

VICTOR TAN and MUSA R. KAMAL, *Department of Chemical Engineering, McGill University, Montreal, P.Q., Canada H3A 2A7*

Synopsis

The properties of injection-molded plastics parts are affected by resin properties, molding geometry, and molding conditions. The thermomechanical history, which results from the interactions between resin properties and molding conditions, controls the development of microstructure within the article. In turn, the microstructure controls the ultimate behavior of injection-molded parts. Morphology and orientation and their distributions are among the most important microstructural characteristics affecting the ultimate mechanical and physical behavior of molded articles. This work summarizes some of the results of an extensive experimental and theoretical program to study the factors affecting the development of morphology and orientation in injection-molded polyethylene. In particular, various experimental techniques are employed to study the distribution of morphology and orientation in simple moldings and to relate these characteristics to resin properties and molding variables. Furthermore, an attempt is made to employ mathematical models to explain and predict some of the observed phenomena especially in relation to the distribution of morphological zones in the molding. It appears that model predictions are in good agreement with experimental results.

INTRODUCTION

A number of workers have attempted to study and model the injection-molding process for thermoplastics.[1–10] Some recent work has concentrated on the study of the morphology and orientation of injection-molded articles.[11–15] For crystalline polymers, it has been found that three morphological regions are discernible.[11–13] These ranged from a nonspherulitic, highly oriented surface layer to a spherulitic, relatively unstrained central core. On the basis of shrinkage measurements, Menges and Wubken[14] have found, in studies with polystyrene moldings, that maximum orientation in the flow direction is attained at the surface. Other maxima are observed as the distance of the microtomed samples from the wall increases approaching the center of the molding. The number and levels of the maxima depend on the position of the sample relative to the gate. However, a general decrease in orientation is observed. Similar results have been reported by Bakerdjian and Kamal[15] on the basis of birefringence measurements in polystyrene moldings. However, the latter workers have observed a more complex behavior in conjunction with polyethylene moldings. The complexity arises from the interaction between orientation and crystallization phenomena.

In this paper we summarize results of work conducted with the aim of elucidating the orientation and morphological effects in polyethylene injection molding. A variety of experimental techniques have been employed, including polarized light microscopy, and infrared measurements in addition to differential scanning calorimetry.

Journal of Applied Polymer Science, Vol. 22, 2341–2355 (1978)

0021-8995/78/0022-2341$01.00

EXPERIMENTAL

Materials

The material used in this study was linear polyethylene Sclair 2911, which was supplied by du Pont of Canada. Moldings were obtained employing a melt temperature of 350°F (175°C) and a mold temperature of 79°F (26°C). A reciprocating-screw, 2⅓-oz. Metalmec injection molding machine was employed to obtain the moldings. A center-gated mold cavity was employed. The dimensions of the rectangular mold were 5 in. × 2.5 in. × 0.0625 in. A typical pressure–time diagram for the gate representing the molding cycle employed in the production of the moldings used in the study is given in Figure 1.

Techniques

Preliminary studies on the distribution of birefringence and density of polyethylene moldings were conducted by Bakerdjian and Kamal.[15] The very complex behavior of birefringence of polyethylene suggests that more elaborate efforts and techniques must be used. For infrared dichroic ratio measurement and thermal characterization, larger rectangular pieces (7.0 mm × 4.0 mm) were cut from the same molding at various positions, as indicated in Figure 2. Sections of 10-micron thickness were sliced in the depth direction (parallel to the surface of the molding) from the above pieces.

In order to examine the distribution of the various morphological features of the molding, samples of 20-micron thickness were also microtomed in the longitudinal direction (XZ plane) and in the transverse direction (YZ plane). A Riechert Zetopan-Pol polarizing microscope was used to take photomicrographs of the longitudinal and transverse cross sections of the various positions, using magnification of 100×. The distribution of spherulite size in the depth direction was determined by visual estimation over a graduated eye piece whose magnification could be accurately calibrated against a microscope slide graduated to 0.01 mm. The magnification used were 350× and 750×.

The dichroic ratio of each section was obtained by a Perkin-Elmer infrared grating spectrophotometer Model 457, with the additional attachment of a sample space wire grid polarizer and a 4× condenser. The beam attenuator was set at 100% transmission at the 700 cm^{-1} band position before the sample was placed in the sample beam. The sample was then placed at 45° to the slit, and

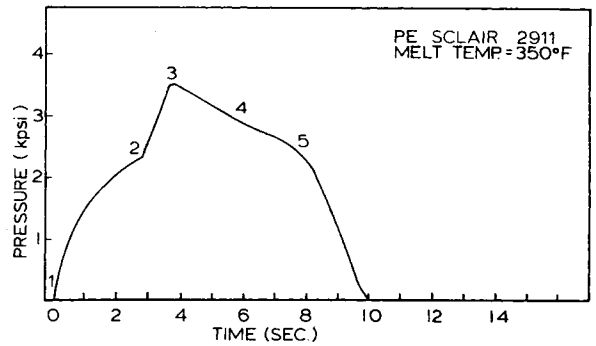

Fig. 1. Pressure traces for transducer located at the gate.

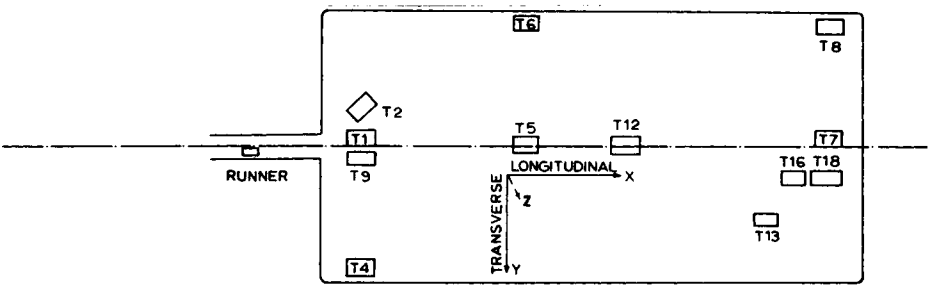

Fig. 2. Positions of various samples cut from the molding to study the variation of properties in the depth direction.

the polarizer was set at the 45° and 315° positions to measure the absorption in the longitudinal (A_L) and the transverse (A_T) direction of the molding, respectively.

The strongest absorption bands of linear polyethylene are listed in Table I together with the interpretation of the crystalline and/or amorphous contributions.[16] The conventional dichroic ratio is defined as $D = A_{\parallel}/A_{\perp}$, where $A_{\parallel}$ is the absorbance measured with radiation polarized parallel to the direction of deformation and $A_{\perp}$ is the absorbance measured with radiation polarized perpendicular to the direction of deformation. This ratio could be converted to the Herman orientation function f; for example, for a-axis orientation of polyethylene, $f_a = (D_{730} - 1)/(D_{730} + 2)$. Without additional information from x-ray diffraction, it is not possible to convert[16] D_{720} into f_b, since the former consists of contributions from both the crystalline and the amorphous phases.

The deformation of the polymers prior to solidification could be quite complex. It could undergo a series of uniaxial, biaxial, or even multiaxial deformations depending on the fluid dynamics of the system. Since there was no attempt to determine the predominant direction of deformation of each microtome section, the dichroic ratio D, which is being measured as $D = A_L/A_T$, could have a magnitude quite different from the conventional dichroic ratio. Hence, no attempt is taken to convert these dichroic ratios into Herman orientation functions.

After the determination of the dichroic ratio, the thermal characteristics of the sections were determined by the differential scanning calorimeter. A Perkin-Elmer DSC Model 1 was used for thermal characterization. The weight of the microtome sections was measured with a Cahn RG electrobalance with accuracy of ±0.001 mg. The calibration was optimized using both benzoic acid and indium at a scan speed of 10°C/min.

TABLE I
Band Assignments of Linear Polyethylene

Frequency, cm^{-1}	Type of vibration of CH_2 group	Contribution	Crystal axis
2919	asymmetric stretching		
2851	symmetric stretching		
1473	bending	crystalline	
1463	bending	crystalline	
		amorphous	
731	rocking	crystalline	a-axis
720	rocking	crystalline	b-axis
		amorphous	

RESULTS AND DISCUSSION

Morphological Observations

The various morphological structures which were developed in the molding are shown in Figure 3. The longitudinal cross section (XZ plane) of various positions with increasing distance from the gate are shown from left to right in the top row and are represented by sample designation as T9, T5, T12, and T18. The transverse cross section (YZ plane) of these positions are shown in the bottom row. The following four distinct morphological zones may be observed in these cross sections.

Type I is a nonspherulitic structure which does not exhibit the Maltese cross pattern. When viewed in the longitudinal cross section (XZ plane) at a magnification of 400×, this zone exhibits tiny slots of vertical bright lines arranged in rows and running parallel to the surface of the molding. The rows are separated by continuous dark bands. They form at the surface/or close to the surface of the molding in the zone commonly referred to as the *skin* of the molding. They may be interpreted as stacks of lamellae with chain axes nucleated in the flow direction and growing in the depth direction.

Type II contains very fine asymmetric spherulites of almost uniform size. These are spherulites that are formed under large thermal gradients and the nucleation rate is very fast, thus limiting the size of the spherulites.

Type III contains asymmetric oblate spherulites with axis of symmetry in the

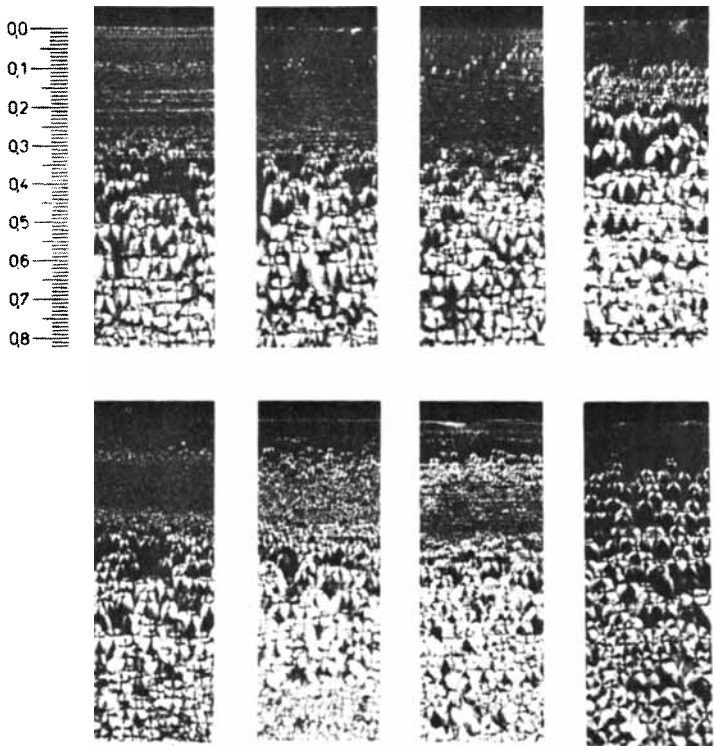

Fig. 3. Morphology of injection-molded polyethylene. Top row: XZ cross sections of positions T9, T5, T12, and T18 (from left to right). Bottom row: YZ cross sections of these positions. The smallest division of the scale is 10 microns.

depth direction, i.e., the direction of the thermal gradient. These spherulites have a higher growth potential, and the growth front is composed of parallel lamallae.[17-19]

Type IV contains randomly nucleated spherulites which grow in all directions until impingement halts growth.

The sequences of formation of these zones from the surface to the central core are not the same throughout the molding. For the region near the gate, the sequence is as follows: types I, II, III, and IV. However, for positions remote from the gate, T5 and T12, and T18, the sequence is different: types II, I, III, and IV. It has been observed that type II structure appears occasionally within the matrix of type I structure. The thickness of each zone varies from position to position.

It was speculated[12] that only one type of structure, type I, was formed during the filling stage of the injection molding process. However, for the polyethylene resin under consideration, it will be shown later that our results indicate that two zones (types I and II) may be formed during the filling stage, while the other two zones (types III and IV) tend to be formed during the packing and the pressure holding stages of the molding cycle.

The zone boundaries and the thicknesses of the four zones can be roughly estimated from the photomicrographs of the transverse cross sections, and they are tabulated in Table II for the various positions investigated.

Spherulite Size

Figure 4 shows the variation of spherulite size with depth at various positions as indicated. Position T4 shows the smallest spherulites at the central core among the positions investigated. This could be attributed to the longer residence time of the stagnant melt and the high packing pressure at this position. At positions T7 and T8, the average spherulite size at the central core is the largest because of the lower packing pressure at the farthest distance from the gate. Since the nucleation rate is not enhanced under lower pressure to the same extent as under high pressure, the spherulites will grow to a larger size until impingement. On the other hand, position T1 near the gate experiences very high shear stresses and fast cooling rates during the early stages of molding. As a result, the nucleation rate is enhanced and types I and II structures are formed.

TABLE II
Variation of Morphological Zones with Distance from the Gate

Sample designation	Distance from surface of molding, microns			
	T9[a]	T5	T12	T18
Type I, nonspherulitic structure	0–80	10–80	20–110	30–100
Type II, small asymmetric spherulites	80–220	0–10 and	0–20 and	0–30
	—	80–330	110–310	—
Type III, oblate asymmetric spherulites	220–550	330–540	310–550	100–580
Type IV, randomly nucleated spherulites	550–950	540–950	550–950	580–950

[a] Designation of positions.

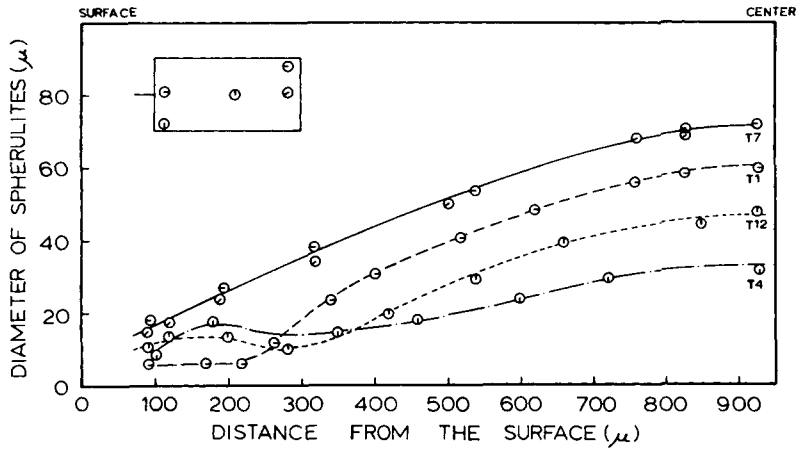

Fig. 4. Variation of spherulites sizes with depth at the various positions as indicated.

At the later stages of molding, position T1 is subjected to the highest packing pressure, but it also has a higher average temperature than the other positions. The net combined effect is that the position near the gate contains larger spherulites than a position at halfway of the molding (T12).

Infrared Measurements

All the results of the dichroic ratio measurements for the CH_2 rocking vibration at the 720 cm^{-1} band absorption, which arises from both the crystalline b-axis and the amorphous phase, are low at the surface, as can be seen in Figures 5, 6, 7, and 8 for positions designated as T1, T4, T12, and T7. This means that the amorphous portions are oriented in the longitudiral direction. However, the crystalline a-axis absorption at the 731 cm^{-1} band leads to a minimum in the dichroic ratio next to the surface, as shown in Figures 6, 7, and 8, except for the position T1 near the gate. Thus, maximum longitudinal orientation appears to occur near the surface. As will be shown later, this is confirmed by differential scanning calorimetry (DSC) measurements.

A value of dichroic ratio lower than 1.0 signifies a preferred orientation in the transverse direction, while a value greater than 1.0 signifies a preferred orientation in the longitudinal direction. Hence, near the surface where both the a-axis and the b-axis show a preferred orientation in the transverse direction, the c-axis must be preferably oriented in the longitudinal direction.

By comparing Figures 6, 7, and 8 with morphological zones of Figure 3, it was found that the positions of a minimum in the a-axis dichroic ratio correspond to the positions where the onset of the nonspherulitic structure is observed. The nonspherulitic structure is considered to be due to flow-induced crystallization of the oriented polymers. The morphology of flow-induced crystallization is that of the row-nucleated lamallae proposed by Keller and Machin[20] and observed in injection-molded parts by Clark.[11,12] According to this model, molecules or segments of molecules are first crystallized in their extended conformations; then these extended chain crystals act as substrates for the growth of parallel or twisted lamallae.

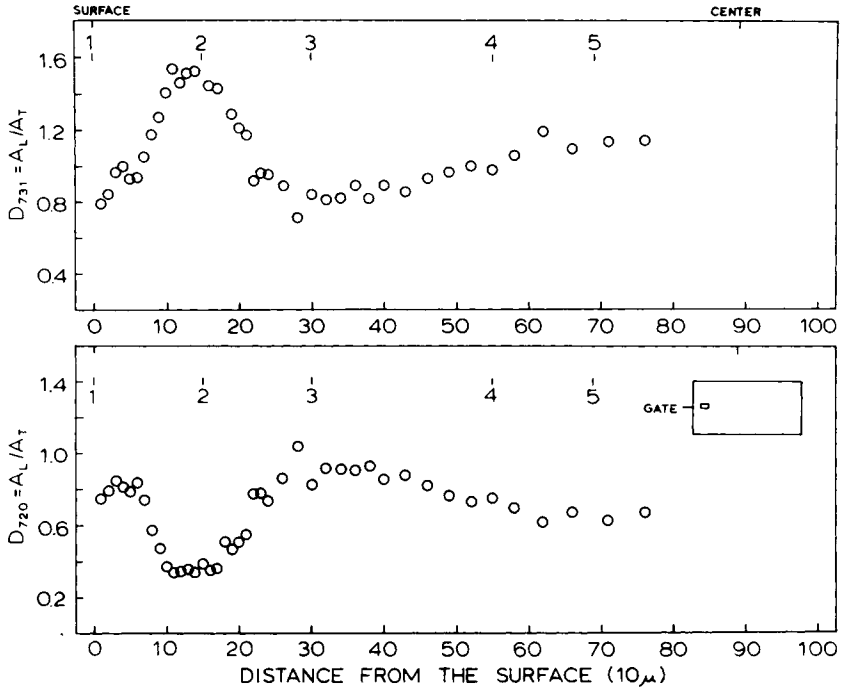

Fig. 5. Variation of infrared dichroic ratio of the 731-cm^{-1} band (top) and 720-cm^{-1} band (bottom) with depth at position located near the gate.

Differential Scanning Calorimetry

The endotherm of an annealed polyethylene sample is shown in Figure 9. A typical endotherm for an unannealed microtome section is shown in Figure 10. On the basis of extensive experimental data, the following observations may be made: (1) The endotherm of an annealed sample peaks at 130°C and ends at 134.5°C. (2) The endotherms for unannealed microtome sections show two peaks: one at 129.5°–130°C and a high-temperature peak at 132.8°–133.5°C. The melting ends at 136°–137°C. (3) The areas under the individual peaks and under the entire endotherm vary from section to section.

The area under the high-temperature peak may be associated with the fraction of the polymer that is crystallized under the effect of orientation.[21] Therefore, the quantity $\dot{Q}_2/\dot{Q}_1$, which is the ratio of the height of the high-temperature peak to that of the low-temperature peak, could be taken as an indirect measure of the ratio of the crystals that have been formed under the influence of orientation to those formed by normal cooling under pressure.

Variation of the quantity $\dot{Q}_2/\dot{Q}_1$ with depth is shown in Figures 11(A), 12(A), 13(A), and 14(A) for sample designated as T1, T4, T12, and T7, respectively. It is quite clear that the highest value of $\dot{Q}_2/\dot{Q}_1$ does not occur at the surface of the molding but at a layer near the surface. This is in agreement with the observation that the maximum orientation of the crystalline a-axis, as measured with the infrared adsorption at 731 cm^{-1}, shows a minimum dichroic ratio at the same position, compare Figures 7 and 13(A).· Inspection of these positions where $\dot{Q}_2/\dot{Q}_1$ exhibits a first maximum reveals that they are the locations associated with the onset of nonspherulitic type I structure for samples taken at the middle of the molding and farthest from the gate. The transverse cross section of sample

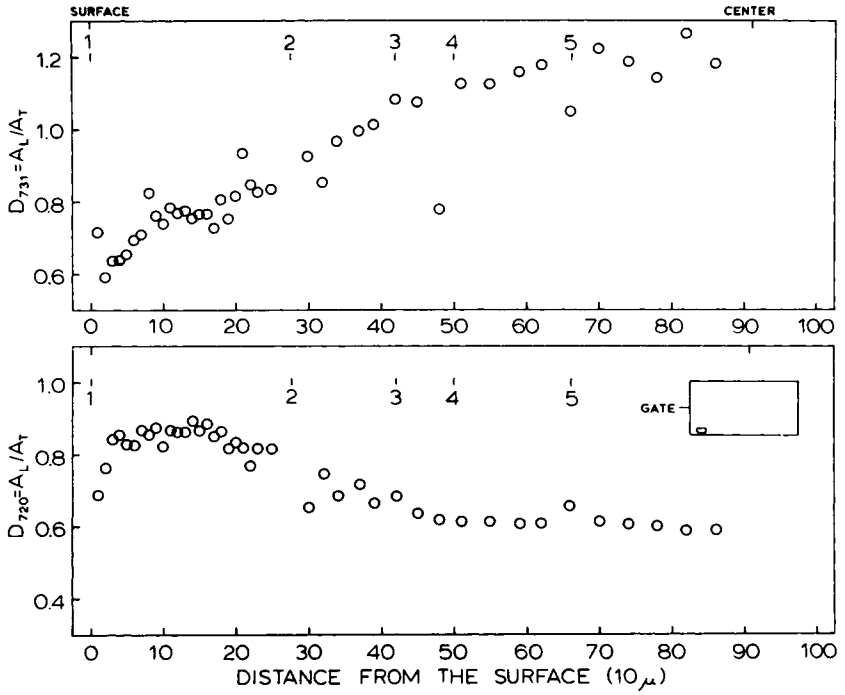

Fig. 6. Variation of infrared dichroic ratio of the 731-cm^{-1} band (top) and 720-cm^{-1} band (bottom) with depth at position located near the corner as indicated.

T5 shows a bright line at the surface. This bright line is not an experimental artifact of microtoming but it consists of a fine layer of type II structure.

It is natural to suspect that the lower value of $\dot{Q}_2/\dot{Q}_1$ at the surface may be associated with the presence of type II structure. Since the value of $\dot{Q}_2/\dot{Q}_1$ is also lower at the surface for position T1 near the gate, an attempt to detect type II structure *at* the surface for this position has revealed only sparse manifestations of this structure, but they do not form an uniform layer.

The different morphological sequences at the various positions may be attributed to the dynamics of melt flow inside the cavity. It has been observed[10] that near the gate, the melt fills the cavity in a radial flow fashion. This radial flow imparts a biaxial deformation to the fluid elements at the melt front,[14] and it may thus introduce sufficient molecular deformation for the nucleation of type I structure. Then lamellar growth can take place under the fast-cooling action of the steel mold. On the other hand, about halfway downstream, the melt fills the mold cavity in a unidirectional fashion with a melt front that is almost straight.[10] It has been observed[14] that the melt element that is frozen at the surface of the molding actually originates from the central core of the advancing melt front where it has experienced relatively little shear deformation. When this melt element solidifies under the fast quenching action of the cold mold, extremely small spherulites are formed. This fine layer of tiny type II spherulites will act as a thermal insulating layer for heat conduction and also serves as the anchoring point for molecular stretching, thus enhancing the formation of type I structure. At position farthest from the gate, the fluid elements that undergo the cooling action of the cold wall have already been cooled slowly along the path; thus, the 30-micron thickness of type II structure at the surface may be an indication of an instantaneous frozen layer.

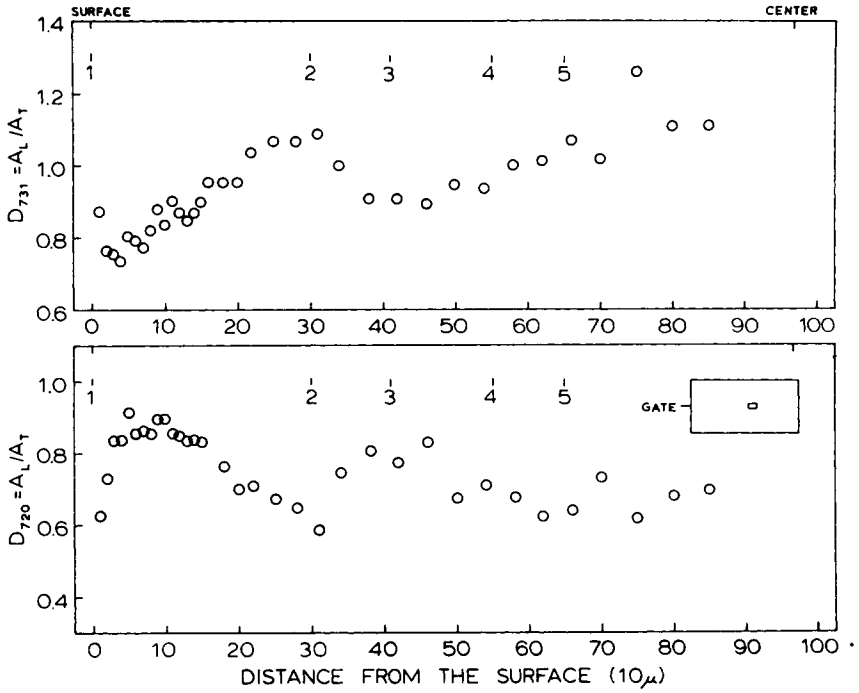

Fig. 7. Variation of infrared dichroic ratio of the 731-cm^{-1} band (top) and 720-cm^{-1} band (bottom) with depth at position located at about the middle of the mold as indicated.

The variation of the heat of fusion with depth at various positions is shown in Figures 11(B), 12(B), 13(B), and 14(B). Near the gate, two or three maxima are observed together with some minima. At halfway of the mold and at the farthest end, the heat of fusion, which reflects the percentage crystallinity, shows a monotonic increase with depth, except for a sudden drop at some distance from the surface.

Comparison of the positions of the first minimum in $\dot{Q}_2/\dot{Q}_1$ with similar data on the heat of fusion, dichroic ratio, and spherulitic size leads to the following observations: (1) At the position of the first minimum in $\dot{Q}_2/\dot{Q}_1$, The heats of fusion exhibit a sudden drop. This indicates the presence of a large fraction of amorphous chains at this point. (2) The first minimum in $\dot{Q}_2/\dot{Q}_1$ is associated with a minimum in the dichroic ratio at 720 cm^{-1}. (3) The beginning of spherulitic growth occurs at the same position as the first minimum in $\dot{Q}_2/\dot{Q}_1$.

It is suggested here that the first minimum in $\dot{Q}_2/\dot{Q}_1$ may be associated with the thickness of the solidifying layer at the time when the cavity is completely filled, i.e., at the end of the filling stage. This time is designated as point 2 in Figure 1, which shows the monitored pressure trace at the gate for the molding of the polyethylene resin under consideration. The thickness of the solidified layer, as estimated from the first minimum in $\dot{Q}_2/\dot{Q}_1$, is tabulated in Table III for the various positions investigated. Comparison of data shown in Tables II and III suggests that two structures, types I and II, are formed during the filling stage.

According to the above observations, the thickness of the solidified layer at the end of the filling stage varies from 160 microns near the gate to 330 microns at the middle of the molding to 175 microns at the far end. The thickness is the

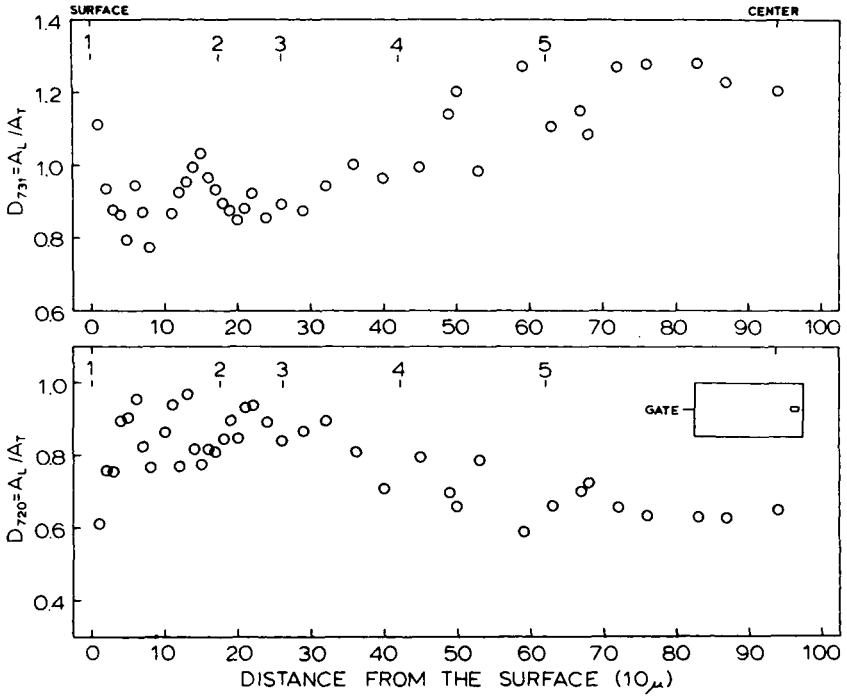

Fig. 8. Variation of infrared dichroic ratio of the 731-cm^{-1} band (top) and 720-cm^{-1} band (bottom) with depth at position located at the farthest end of the mold as indicated.

lowest near the gate due to the relatively high temperature throughout the filling stage in that region. The thickness is low at the far end, when filling is completed, as a result of the short contact time between the polymer reaching that end and the cavity wall. The thickness is large in the middle of the molding due to the long cooling time experienced by the polymer in that region.

The decreasing nature of $\dot{Q}_2/\dot{Q}_1$ for layers starting near the surface and moving away from the wall toward the first minimum in the $\dot{Q}_2/\dot{Q}_1$ versus-depth curve may be due to the decreasing shear stress during the filling stage in these layers. In fact, preliminary computer simulation of the mold-filling process shows that

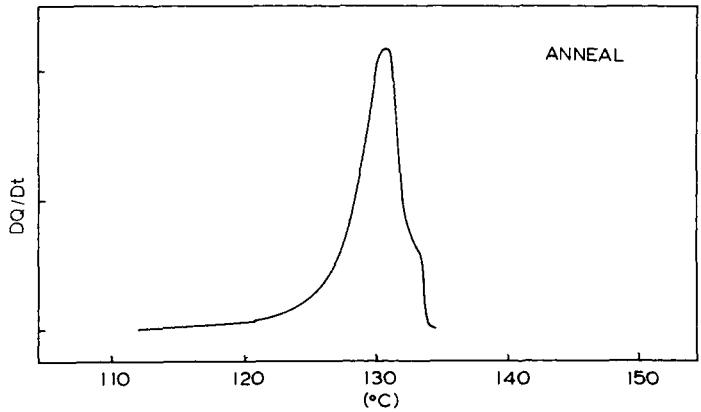

Fig. 9. DSC endotherm for a sample annealed at 100°C for 18 hr.

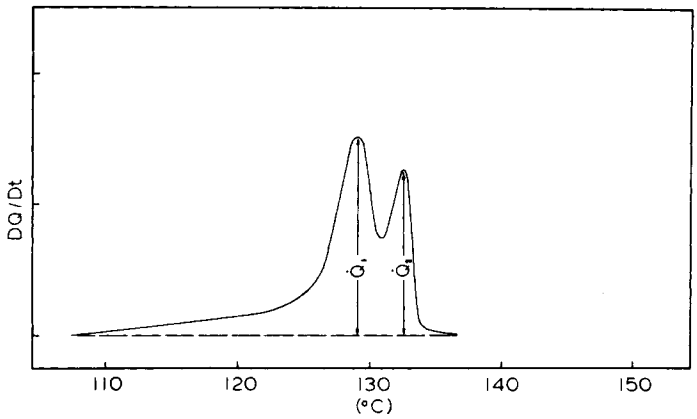

Fig. 10. DSC endotherm for microtome section at the surface of the molding.

this is indeed the case. The results of the computer simulation will be reported elsewhere.

Other maxima in $\dot{Q}_2/\dot{Q}_1$ have been observed to exist at moderate distances from the wall. Comparison of the position of the second maximum in $\dot{Q}_2/\dot{Q}_1$ with data from other measurements, with due consideration to the pressure–time curve for the process, suggests that the second maximum may be associated with the completion of the packing stage, which has been designated as point 3 in Figure 1. The details of the flow patterns in the cavity during the packing stage are rather complex. However, it is obvious that the fluid elements immediately near the solid–melt interface will experience relatively excessive shear deformation

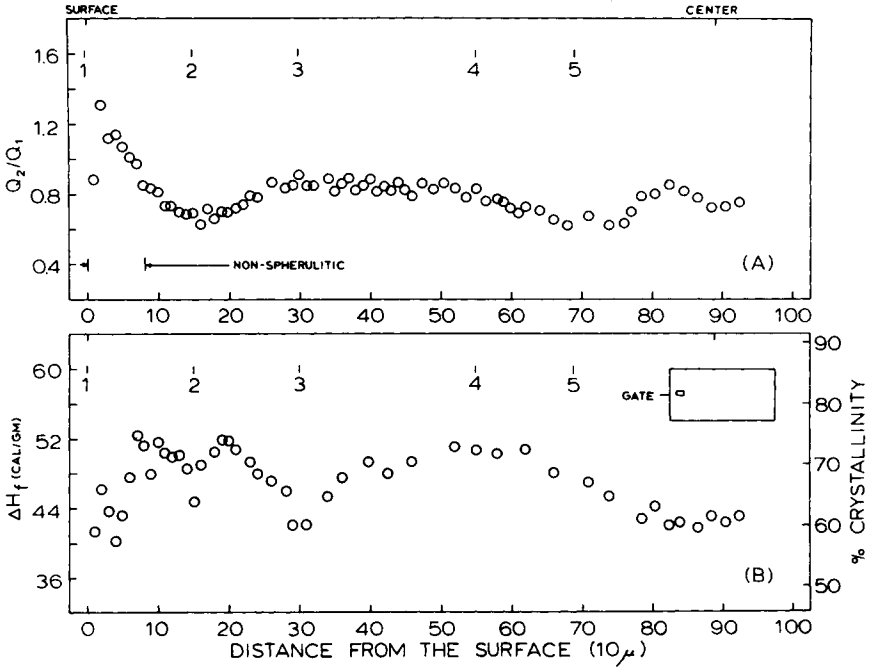

Fig. 11. Variation of (A) the quantity $\dot{Q}_2/\dot{Q}_1$ and (B) heat of fusion, with depth at position located near the gate.

TABLE III
Estimated Thickness of Solidified Layer at Various Positions

Sample designation	Distance from surface of molding, microns						
	T1	T2	T4	T5	T12	T16	T7
Position of the solid–melt interface at:							
1. Instantaneous frozen layer (speculated)	—	—	—	10	20		30
2. Completion of filling (2.6 sec)	160	210	275	330	310	215	175
3. The highest packing pressure (3.5 sec)	300	375	420	430	410	320	260
4. The time which additional in-flow of melt was observed during the pressure holding period (5.6 sec)	510	500	500	540	550	520	420

due to the requirement of no-slip at this interface. Accordingly, melt elements near this interface will exhibit higher molecular orientation.

The thickness of the solidified layer at the end of the packing stage, as deduced from $\dot{Q}_2/\dot{Q}_1$ data according to the above hypothesis, is shown in Table III for the various positions included in the present study.

The pressure–time curve for the molding under study, Figure 1, shows an inflection point during the cooling stage. This inflection, designated as region 4, may be attributed to the additional in-flow of the melt before the fluid elements near the gate are frozen completely. The additional flow of the melt gives rise to another maximum in $\dot{Q}_2/\dot{Q}_1$ as indicated in region 4 of Figure 11(A). However, the exact location of this region could not be ascertained with great accuracy. It is believed that the type IV morphological zone starts to develop at this time.

Table III summarizes the estimated thickness of the solidified layer associated

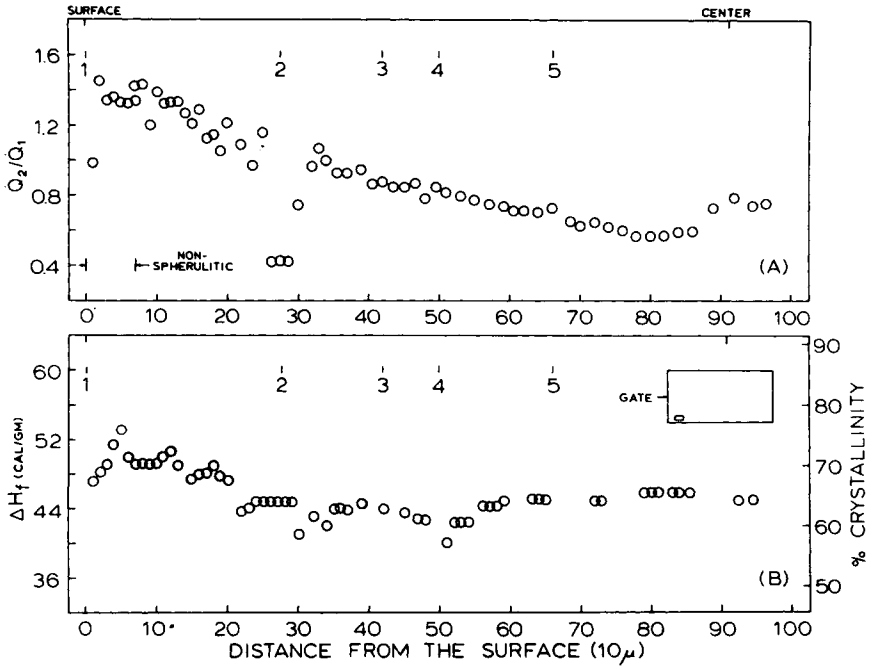

Fig. 12. Variation of (A) the quantity $\dot{Q}_2/\dot{Q}_1$ and (B) heat of fusion, with depth at position located at the corner as indicated.

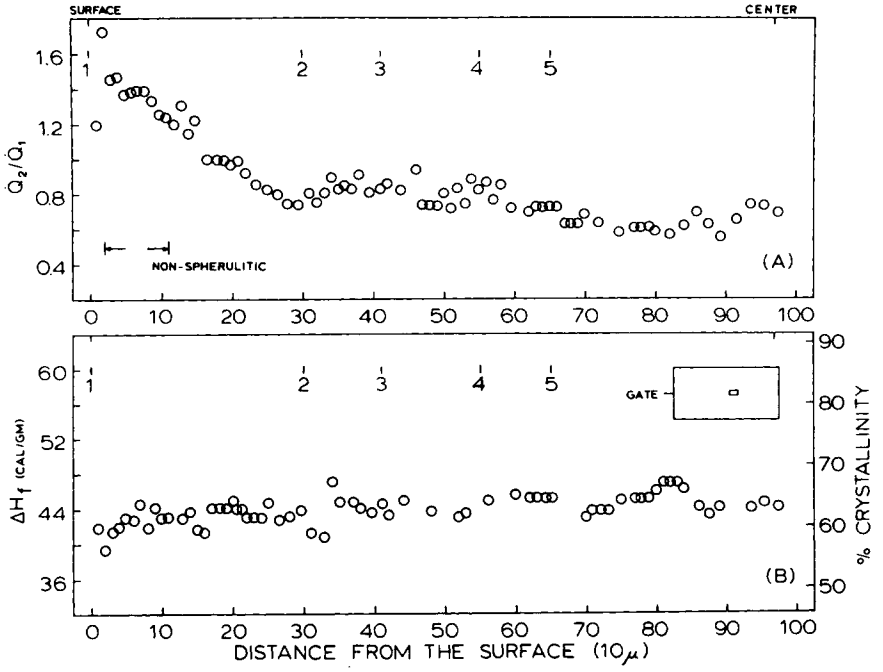

Fig. 13. Variation of (A) the quantity $\dot{Q}_2/\dot{Q}_1$ and (B) heat of fusion, with depth at position located at about the middle of the mold as indicated.

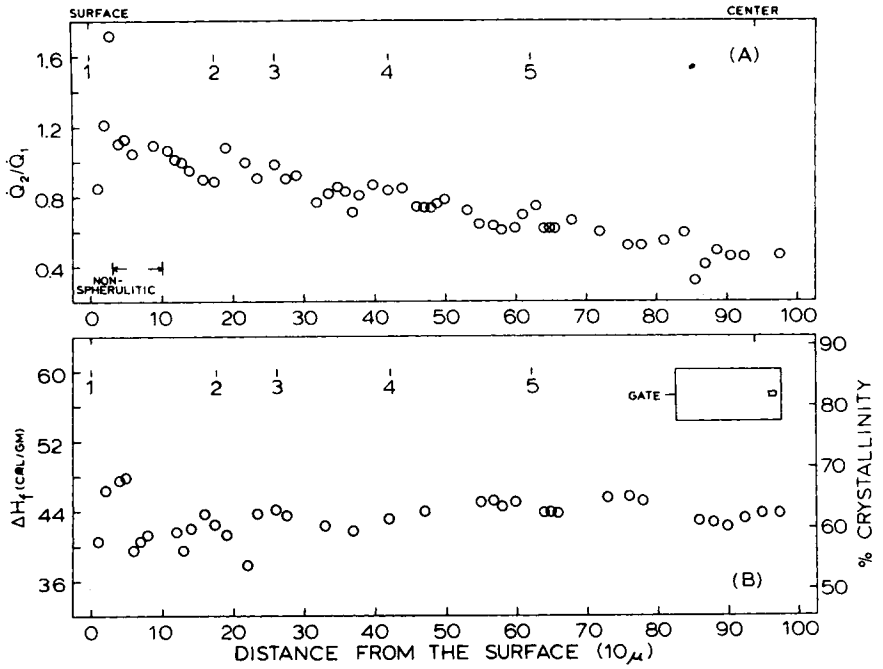

Fig. 14. Variation of (A) the quantity $\dot{Q}_2/\dot{Q}_1$ and (B) heat of fusion, with depth at position located at the farthest end of the mold as indicated.

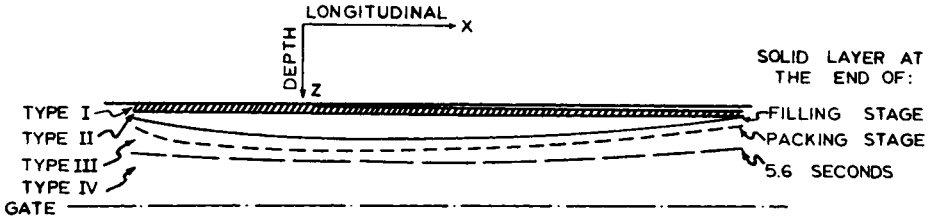

Fig. 15. Thickness of the solid layer at various stages of the injection molding process. Solid line for the filling stage; short broken line for the packing stage; long broken line for the pressure-holding stage. Shaded area is the region of nonspherulitic type I structure.

with the various stages of the molding process at the positions investigated. These values are also plotted in Figure 15 as a cross-sectional view along the longitudinal direction. This trend in solid skin development is in agreement with the predictions of various workers.[22,23] Figure 16 shows the thickness of the solid layer at various stages of the molding process as predicted by computer simulation. Good agreement is obtained between the computer model and experimental observations, within the framework of the above hypotheses. The deviations near the gate are not surprising due to the complexity of the boundary conditions in that region.

Inside the mold cavity, all positions which have been investigated exhibit the same trend for the variation in the quantity $\dot{Q}_2/\dot{Q}_1$. However, in the runner, only type II morphology has been observed, and only little orientation of the frozen layer at the surface is indicated, as can be seen in Figure 17. This observation could not be explained in terms of one-dimensional shear flow or by fountain flow involving elongational deformations.[24] In order to explain the behavior in the runner, it may be necessary to obtain a precise mathematical solution of the fluid flow near the melt front.

CONCLUSIONS

In this work a variety of techniques have been employed to study the distribution of orientation and morphological stress in injection-molded articles made from polyethylene. The nature of these distributions has been related to some of the critical flow and thermal phenomena occurring during the molding process. In particular, the development of four distinct morphological zones, the devel-

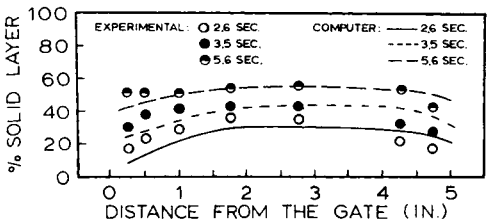

Fig. 16. Comparison of solid layer as measured experimentally and that predicted by computer models at the end of filling stage (2.6 sec), packing stage (3.5 sec), and at pressure holding stage (5.6 sec).

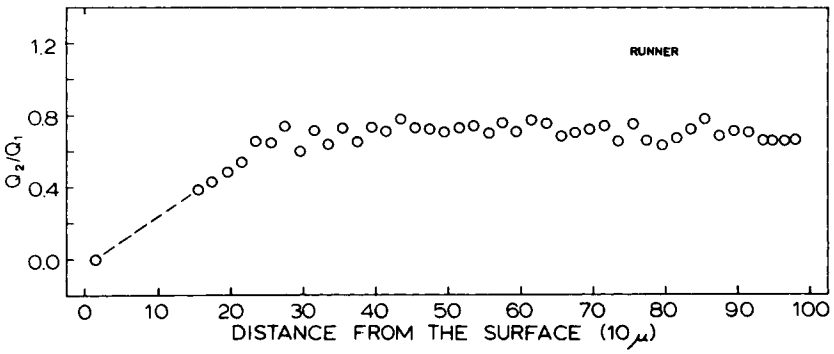

Fig. 17. Variation of the quantity $\dot{Q}_2/\dot{Q}_1$ with depth at position located at the runner.

opment of orientation in the various zones, and the growth of the solid layer next to the wall have been explained qualitativity in terms of such flow and thermal phenomena. The results and the proposed explanations of these results appear to be in good agreement with the predictions of computer simulation.

The authors wish to thank Professor R. St. John Manley of the Pulp and Paper Research Institute of McGill University for helpful discussions regarding the morphology of polyethylene.

References

1. R. S. Spencer and G. D. Gilmore, *Mod. Plast.*, **28**, 97 (December 1950).
2. R. S. Spencer and G. D. Gilmore, *J. Colloid Sci.*, **6**, 118 (1951).
3. G. D. Gilmore and R. S. Spencer, *Mod. Plast.*, **28**, 117 (April 1951).
4. F. J. Reilly and W. L. Price, *SPE J.*, **17**, 1097, October (1961).
5. D. H. Harry and R. G. Parrot, *Polym. Eng. Sci.*, **10**, 209 (1970).
6. J. L. Berger and C. G. Gogos, *Polym. Eng. Sci.*, **13**, 107 (1973).
7. M. R. Kamal and S. Kenig, *Polym. Eng. Sci.*, **12**, 294 (1972).
8. M. R. Kamal and S. Kenig, *Polym. Eng. Sci.*, **12**, 302 (1972).
9. S. Kenig, Ph.D. Thesis, McGill University, Montreal, 1972.
10. P. H. Doan, M. Eng. Thesis, McGill University, Montreal, 1974.
11. E. S. Clark, *Plast. Eng.*, **30**(4), 73 (1974).
12. E. S. Clark, *Polym. Prepr.*, **14**(1), 268 (1973).
13. M. R. Kantz, H. D. Newman, Jr., and F. H. Stigale, *J. Appl. Polym. Sci.*, **16**, 1249 (1972).
14. G. Menges and G. Wubken, *SPE ANTEC*, **19**, 519 (1973).
15. Z. Bakerdjian and M. R. Kamal, *SPE ANTEC*, **21**, 297 (1975).
16. R. S. Stein, *Macromolecules*, **1**, 116 (1968).
17. A. J. Lovinger and C. C. Gryte, *Macromolecules*, **9**, 247 (1976).
18. A. J. Lovinger, C. M. Lau, and C. C. Gryte, *Polymer*, **17**, 581 (1976).
19. D. Hansen, A. N. Taskar, and O. Casale, *J. Appl. Polym. Sci.*, **10**, 1615 (1972).
20. A. Keller and M. J. Machin, *J. Macromol. Sci. Phys.*, **B1**(1), 41 (1967).
21. V. Tan and C. G. Gogos, *Polym. Eng. Sci.*, **16**, 512 (1976).
22. H. A. Lord and G. Williams, *Polym. Eng. Sci.*, **15**, 569 (1975).
23. C. Gutfinger, E. Broyer, and Z. Tadmor, *Polym. Eng. Sci.*, **15**, 515 (1975).
24. Z. Tadmor, *J. Appl. Polym. Sci.*, **18**, 1953 (1974).

Received January 21, 1977
Revised May 11, 1977